

Inviscid vortex breakdown models in pipes

R. Fernandez-Feria and J. Ortega-Casanova

Abstract. The inviscid evolution along a pipe of two families of inlet cylindrical swirling flows is analysed using the Bragg-Hawthorne equation. The first flow corresponds to exact solutions of the axisymmetric Euler equations near the axis, at which the velocity field is singular. The quasi-cylindrical problem is reduced to solving a phase-plane first order differential equation. It is found that, for both converging and diverging pipes, cylindrical solutions for the downstream flow determined by the inlet flow exist even for very high values of the swirl parameter (L). The second family of inlet flows coincides with the first except inside an axial core of radius r_c , where the flow now has constant axial velocity and rotates as a rigid body. For diverging or straight pipes, this regularised family exhibits the usual behaviour, with a maximum value of $L = L_f$ above which one-cell cylindrical solutions for the downstream flow fail to exist, even for very small r_c . The downstream flow may also stagnate at the axis above another value $L_o < L_f$. Thus, there is no inviscid breakdown unless the vortex core is (arbitrarily) regularised. Since regularization of singular inviscid flows is actually carried out by viscosity, it follows that, within the limitations of the present simple model, the presence of viscosity is essential to describe the phenomenon of vortex breakdown in pipes from the inviscid equations, regularising the usually singular inlet inviscid flow. The jet-like radial decay of the axial and swirl velocities in the present inlet model flows leads also to values of L_f closer to those observed experimentally than those found in some previous models.

Keywords. Swirling flows, vortex breakdown, phase-plane analysis.

1. Introduction

The phenomenon of vortex breakdown, particularly in pipes, has usually been described and explained by inviscid equations and arguments (e.g. [1]-[6]). Most of these works considered the *inviscid* evolution of a particular inlet swirling flow along a pipe of given geometry using the Bragg-Hawthorne (also called Squire-Long) equation (see next section). The velocity profile most used to simulate the inlet flow in the pipe has been an uniform axial velocity combined with a rigid body rotation (azimuthal velocity linear with the distance to the axis r), or with a Rankine vortex, where the rigid body rotation is confined in a slender core surrounded by a potential vortex (azimuthal velocity inversely proportional to r). More realistic, Gaussian-like, inlet velocity profiles have been considered in [5]. Depending on the pipe geometry and on the type of inlet flow considered, it is

found that, when the relative intensity of the swirl is above a certain threshold, usually expressed in terms of a swirl parameter or Squire number, or its inverse, a Rosby number, the inviscid downstream flow presents several characteristics which are commonly associated to the vortex breakdown phenomenon, or, simply, the equations fail to give a solution for the downstream flow. A simplified version of the problem, first considered by Batchelor [2], and which is the one used in this paper, consists on looking for *cylindrical* solutions of the equations for a given radius of the pipe far downstream, given a cylindrical inlet velocity profile. Although this formulation does not yield the velocity field connecting the inlet and outlet flows, it has the important advantage of its simplicity, allowing for analytical solutions in many cases. When the equations fail to yield a cylindrical solution downstream, i.e. when the downstream flow cannot be described by the class of cylindrical velocity profiles looked for, it is assumed that breakdown of the inlet flow occurs. The disadvantage of the method is that one cannot know exactly what really happened to the flow as the pipe radius varied from its inlet value to the outlet one when no cylindrical solution downstream existed; but it suffices for the main purpose of this paper, which is to know whether some families of inlet velocity profiles are, or are not, able to *suffer* breakdown. Nonetheless, in order to check the cylindrical results, and to corroborate the appearance of vortex breakdown when no cylindrical solution exists, we also give some numerical results of the non-cylindrical Bragg-Hawthorne (B-H) equation for some representative cases.

A common feature of all previous inviscid flow simulations is that the inlet velocity fields considered were regular at the axis. However, Euler equations are more likely to yield solutions singular at the axis of symmetry for swirling flows (e.g. the potential vortex, or the more general class of conically similar solutions to Euler equations, proportional to an arbitrary negative power of r near the axis [7]). In general, this situation occurs when an inviscid streamline with non-vanishing circulation coming from the vortex generator (e.g. from the surface of the swirling hub of a vane swirl apparatus) reaches the axis of symmetry: the inviscid conservation of the circulation along streamlines yields an infinite azimuthal velocity at the axis. These singular behaviours are, of course, regularised by viscosity in a narrow axial layer, which constitutes the sometimes called vortex core (e.g. Long's vortex [8], regularising a potential vortex, or the near-axis viscous layer regularising the more general class of conically similar inviscid vortices [7]). In most of the works on the subject, the inlet vortex was arbitrarily regularised at the axis through a core where, as already mentioned, the flow has a constant axial velocity and rotates as a rigid body, which is a rough approximation to the actual behaviour of the viscous flow near the axis. One may question on the correctness of using these regularised inlet velocity profiles in a purely inviscid formulation. Mathematically it is formally correct, because any *cylindrical flow*, i.e. any flow in which the radial velocity is zero, and the azimuthal and axial velocities depend only on r , is a solution to Euler's equations [2]. Thus, all the inlet cylindrical flows considered previously, such as the Rankine's vortex just mentioned, or the

Gaussian-like velocity profiles (which resembles more the *real viscous* velocity profiles), are compatible with the inviscid equations governing the flow inside the pipe, provided that the inlet radius is constant during a certain length. Even if one uses a viscous velocity profile for the inlet flow, for instance, that given by a singular inviscid flow regularised at the axis through a viscous boundary layer, it is compatible with the inviscid equations provided that it is cylindrical. Given this, the other question one may ask is whether the vortex breakdown phenomenon in pipes predicted and described with the inviscid equations is related to the regularization of the inlet velocity profile, and therefore needs the indirect action of viscosity. To answer this question in general is difficult. Numerical viscous simulations for swirling flows inside a pipe have been carried out by Beran and Culik [9], Lopez [10], and Darmofal [11], among others, using Gaussian-like vortices ([9]-[10]), and experimentally fitted velocity profiles ([11]), to model the inlet flow. These authors found that vortex breakdown actually occurs above a critical value of the swirl number of the inlet flow, in agreement with experimental results on vortex breakdown in pipes. Beran and Culik also found that vortex breakdown is related to the failure of the boundary layer equations governing the viscous core of the vortex, thus supporting the *viscous* theory first proposed by Hall [12]. Similar results were reported in [7] for self-similar viscous vortex cores, where the governing near-axis boundary layer equations failed to give a solution above a critical swirl number. Thus, these results add support to the view that vortex breakdown is a phenomenon in which viscosity plays an important role. In this context, the present paper proposes a simpler exercise: to compare the inviscid evolution in a pipe of two families of inlet cylindrical velocity profiles, one singular at the axis, and the other one regularised at the axis in the usual way of assuming a constant axial velocity and a rigid body rotation inside a slender vortex core. As mentioned above, we shall use the cylindrical approximation and find that, for the singular inlet velocities, a downstream cylindrical solution is always found for the most interesting cases so that vortex breakdown is not observed. On the other hand, for the regularised velocity profiles, we reproduce previous results: vortex breakdown occurs for diverging pipes above a critical value of the swirl parameter characterising the inlet flow.

2. The quasi-cylindrical problem

Consider the axisymmetric, steady flow of an inviscid fluid in cylindrical-polar co-ordinates (r, θ, z) , with velocity field (u, v, w) . The stream function for the meridional motion Ψ ,

$$u = -\frac{1}{r} \frac{\partial \Psi}{\partial z}, \quad w = \frac{1}{r} \frac{\partial \Psi}{\partial r}, \quad (1)$$

satisfies the Bragg-Hawthorne [13] equation (also called Squire-Long equation):

$$\frac{\partial^2 \Psi}{\partial r^2} - \frac{1}{r} \frac{\partial \Psi}{\partial r} + \frac{\partial^2 \Psi}{\partial z^2} = r^2 \frac{dH}{d\Psi} - C \frac{dC}{d\Psi}, \quad (2)$$

where $H(\Psi)$ and $C(\Psi)$ are the Bernoulli function and the circulation, respectively:

$$H = \frac{p}{\rho} + \frac{1}{2}(u^2 + v^2 + w^2), \quad C = rv. \quad (3)$$

We shall consider the inviscid flow in a converging or diverging pipe, assuming that far upstream and far downstream the flow is *cylindrical*; i.e. $u = u_z = \Psi_{zz} = 0$. In these cylindrical regions, Eq. (2) becomes

$$\Psi_{rr} - \frac{1}{r} \Psi_r = r^2 H_\Psi - C C_\Psi, \quad (4)$$

where $0 \leq r \leq r_1$ at the inlet, and $0 \leq r \leq r_2$ at the outlet. Given an inlet cylindrical flow, which defines the functions $H(\Psi)$ and $C(\Psi)$, we shall follow Batchelor [2] in solving (4) to obtain the cylindrical flow far downstream, provided that it exits. Batchelor solved it for two cases: a far upstream flow with uniform axial velocity and rotating as a rigid body, and the same flow but considered as an isolated vortex immersed inside a potential vortex. The class of inlet flows was extended by Buntine and Saffman [5], who also considered Gaussian-like inlet velocity profiles (sometimes called q-vortices). We shall consider in the next section a family of inlet flows with velocity fields proportional to a negative power of the distance to the axis, $(v, w) \sim r^{m-2}$, $1 \leq m < 2$, which correspond to exact near-axis solutions to the Euler equations [7]. These inviscid flows are singular at the axis, and will be shown in section 3 to suffer no vortex breakdown for any value of the swirl parameter (for $m = 1$). A second family of inlet flows, now regular at the axis, is considered in section 4. It coincides with the previous one, except in a core of radius r_c , where the flow is assumed to have constant axial velocity and rotates as a rigid body. Thus, the inlet flow is similar to the second type considered by Batchelor, but with an outer axial velocity more like a jet, with a profile proportional to a negative power of r instead of an uniform axial velocity profile everywhere. We shall see that vortex breakdown occurs in the regularised vortex for a *folding* value of the swirl parameter, as also observed by Batchelor [2]. However, the radial decay of the axial velocity outside the vortex core yields values of the folding swirl parameter more in accordance with the observed critical swirl numbers for actual vortex breakdown in pipes.

3. An inlet inviscid flow singular at the axis

Consider the following inviscid flow far upstream ($0 \leq r \leq r_1$, where r_1 is the inlet pipe radius):

$$\Psi = \frac{W_o}{m} r^m; \quad w = W_o r^{m-2}, \quad u = 0; \quad (1 \leq m < 2) \quad (5)$$

$$v = L W_o r^{m-2}, \quad \frac{p}{\rho} = \frac{(L W_o)^2}{2(m-2)} r^{2(m-2)} + \frac{p_o}{\rho}. \quad (6)$$

Functions C and H are given by:

$$C = K \Psi^{(m-1)/m}, \quad K \equiv L(m^{m-1} W_o)^{1/m}, \quad (7)$$

$$H = K_1 \Psi^{2(m-2)/m}, \quad K_1 \equiv \frac{1}{2} \left(1 - \frac{m-1}{2-m} L^2 \right) W_o^{4/m} m^{2(m-2)/m}. \quad (8)$$

Substituting into (4),

$$\Psi_{\eta\eta} = \frac{2(m-2)}{m} K_1 \Psi^{1-4/m} - \frac{m-1}{2m} \frac{K^2}{\eta} \Psi^{1-2/m}, \quad (9)$$

where

$$\eta = r^2/2, \quad (10)$$

and $\Psi_{\eta\eta} = \partial^2 \Psi / \partial \eta^2$. This equation must be solved with the boundary conditions that the axis and the pipe wall are streamlines:

$$\Psi(\eta = 0) = 0, \quad \Psi(\eta = r_2^2/2) = (W_o/m) r_1^m, \quad (11)$$

where r_2 is the outlet radius of the pipe. In terms of the dimensionless stream function $g(\eta)$,

$$\Psi \equiv \frac{W_o L^m}{m} (\eta g)^{m/2}, \quad (12)$$

and defining

$$G \equiv \eta \frac{dg}{d\eta}, \quad (13)$$

equation (9) becomes the first order differential equation

$$\frac{dG}{dg} = \frac{D - (m-1)g + \frac{2-m}{2}(g^2 + G^2) + (1-m)gG}{gG}, \quad (14)$$

where the dimensionless parameter D is given by

$$D = -\frac{4m^2(2-m)K_1}{K^4} = \frac{2}{L^2} \left(m-1 - \frac{2-m}{L^2} \right). \quad (15)$$

With these new variables, the axial and azimuthal velocities are given by

$$w = \frac{W_o L^m}{2} (\eta g)^{(m-2)/2} (G + g), \quad (16)$$

$$v = \frac{W_o L^m}{\sqrt{2}} \eta^{(m-2)/2} g^{(m-1)/2}. \quad (17)$$

A complete phase plane analysis of (14) is given in the appendix. As shown there, the axis corresponds to the singular point ($G = 0, g = 2/L^2$), while the pipe wall, according to (11)-(12), corresponds to $g = 2/(LR)^2$, where

$$R = \frac{r_2}{r_1}. \quad (18)$$

Therefore, there are three non-dimensional parameters governing the present problem: m and L defining the incoming flow, and the expansion ratio R . We shall consider separately first the case $m = 1$ because a simple analytical solution exists.

3.1. $m = 1$

For $m = 1$, equations (14)-(15) become linear in G^2 :

$$\frac{dG}{dg} = \frac{D + \frac{g^2}{2} + \frac{G^2}{2}}{gG}, \quad D = -\frac{2}{L^4} \quad (m = 1). \quad (19)$$

The solution satisfying the first boundary condition (11) at the axis goes through the singular point ($G = 0, g = 2/L^2$), which is a saddle, with positive slope (see appendix):

$$G = g - \frac{2}{L^2}. \quad (20)$$

Substituting into (13) and using the second boundary condition (11), one obtains

$$g = \frac{2}{L^2} \left[1 + \frac{1 - R^2}{R^2} \frac{2\eta}{r_2^2} \right]^{1/2}. \quad (21)$$

In terms of the original variables, the downstream solution is ($0 \leq r \leq r_2$):

$$\Psi = W_o r \left[1 + \frac{1 - R^2}{R^2} \left(\frac{r}{r_2} \right)^2 \right]^{1/2} \quad (m = 1), \quad (22)$$

which yields, according to (1) and (7),

$$w = \frac{W_o}{r} \frac{1 + 2 \frac{1 - R^2}{R^2} \left(\frac{r}{r_2} \right)^2}{\left[1 + \frac{1 - R^2}{R^2} \left(\frac{r}{r_2} \right)^2 \right]^{1/2}}, \quad v = \frac{L W_o}{r}. \quad (23)$$

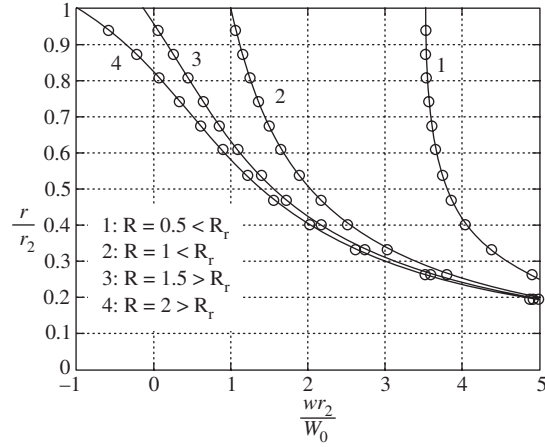


Figure 1.

Downstream axial velocity profiles (r/r_2 vs. wr_2/W_o) for singular inlet flows with $m = 1$, for several values of $R = r_2/r_1$. When $R > \sqrt{2} = R_r$ the axial velocity at the wall becomes negative. The circles correspond to numerical results from the non-cylindrical B-H equation (2) with (7)-(8) for $m = 1$ at $x = 10r_2$.

The azimuthal velocity profile remains unchanged along the pipe, but this is only true for this particular case $m = 1$, for which the circulation C is constant everywhere.

The most important physical feature of the above solution is that the near-axis flow preserves its singularity of the form $(w, v) \sim 1/r$ downstream, independently of the value of the swirl parameter L , so that inviscid vortex breakdown does not occur for any value of L . At the wall ($r = r_2$), the axial velocity increases for a converging pipe, $R < 1$, and decreases for a diverging one, $R > 1$. In the last case, the axial velocity becomes zero at the wall when $R = \sqrt{2}$, and negative when $R > \sqrt{2}$ (see figure 1). Therefore, a zone of flow reversal appears near the wall of the pipe when its radius r_2 is larger than $\sqrt{2}r_1$. Obviously, when this occurs the above solution is not the only possible one, because different functions $H(\Psi)$ and $C(\Psi)$ may be specified in the B-H equation for the backflow coming from the pipe outlet. In other words, for $R > \sqrt{2}$, there exists a region $r^* < r < r_2$ where the downstream function takes values larger than W_o , and therefore outside the interval $[0, W_o]$ in which the functions $H(\Psi)$ and $C(\Psi)$ have been defined upstream. The solution is thus not unique, but depends on the form of these functions for the backflow. The particular solution given for $R > \sqrt{2}$ corresponds to an extension of the same functions $H(\Psi)$ and $C(\Psi)$ of the incoming flow, equations (7)-(8), for $\Psi > W_o$.

To check the different cylindrical solutions to the B-H equation given in this and the following sections, we have also solved the non-cylindrical B-H equation

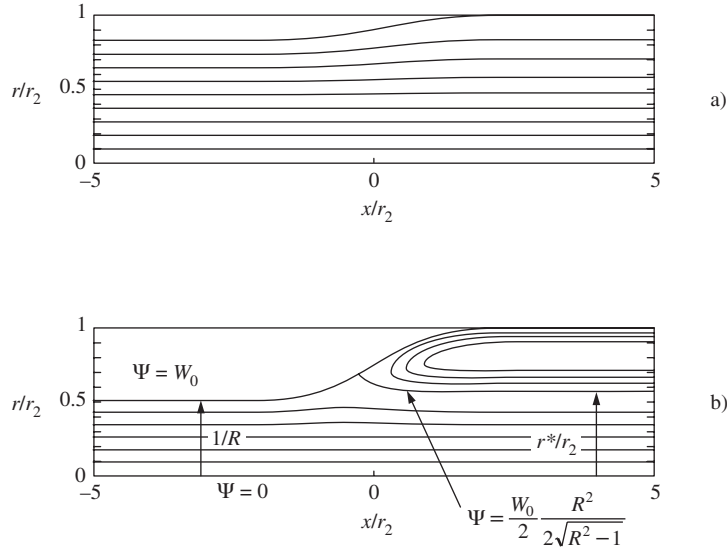


Figure 2. Streamlines obtained numerically by solving (2) with (7)-(8) for $m = 1$ when $R = 1.2$ (a), and $R = 2$ (b).

(2) numerically. The pipe radius used in the computations has the form

$$\frac{r_c(x)}{r_2} = \frac{1}{2} \left[1 + \tanh \frac{x}{r_2} + \frac{1}{R} \left(1 - \tanh \frac{x}{r_2} \right) \right], \quad (24)$$

where R is the expansion ratio of the pipe (18). At the pipe inlet (which is taken $x/r_2 = -10$), the stream function is given by (5) in the present case of an inlet flow singular at the axis. At the pipe outlet ($x/r_2 = 10$), we impose $\partial^2 \Psi / \partial x^2 = 0$. The boundary condition at the axis is $\Psi = 0$, while at the pipe wall, $r = r_c(x)$, Ψ is given by its upstream value at $r = r_1$. The integration domain is first transformed into a rectangle, and finite differences are used in a mesh of 200 equidistant points along the x -direction, and 300 points in the r -direction. The resulting non-linear equation is solved iteratively, using the inlet flow as the initial guess.

For the present upstream inviscid flow singular at the axis with $m = 1$, the results are plotted in figures 1 and 2. The numerical results for the outlet axial velocity profiles at $x = 10r_2$ (circles in figure 1) are indistinguishable from the cylindrical axial velocity profiles given by (23). Figure 2 shows streamlines obtained numerically for two diverging pipes, one with an expansion ratio less than $\sqrt{2}$, and another one with $R > \sqrt{2}$. In the last case, a region of flow reversal is formed near the wall, where the downstream radius r^* separating it from the region of forward axial flow is given with great accuracy by the value of r that maximises w in (23).

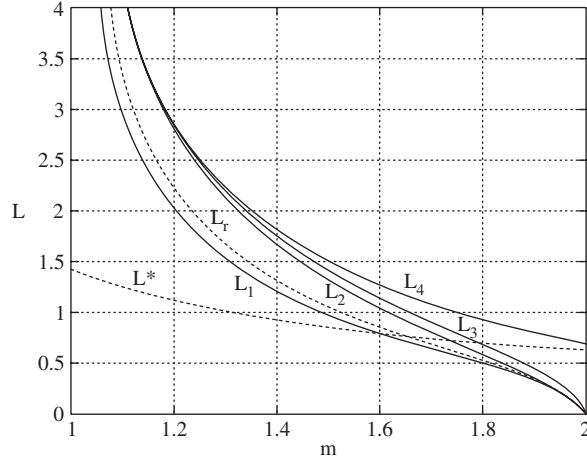


Figure 3. Different distinguished values of the swirl parameter as a function of m . L^* is the critical swirl parameter found in [7], above which no near-axis boundary layer solutions exist.

3.2. $1 < m < 2$

For $m \neq 1$ the problem is richer than for $m = 1$, existing different types of solutions in different regions of the (m, L, R) parametric space. Following the detailed phase-plane analysis given in the appendix, we describe next the main features of these solutions.

It is found (see appendix) that, for each m , a limiting value of the swirl parameter $L_3(m)$ exists,

$$L_3(m) = \sqrt{\frac{2(2-m)}{m-1}}, \quad (25)$$

above which the problem of a diverging pipe has no solution. For the present model of inviscid flows, this limiting value resembles a critical swirl parameter for vortex breakdown, but with the particularity that for a converging or straight pipe a solution always exists (note that L_3 goes to infinity for $m = 1$, so that, as seen above, there is no limiting swirl parameter in the case $m = 1$). This maximum value for the existence of quasi-cylindrical solutions is plotted in figure 3 along with several other distinguished values of the swirl parameter, $L_i(m)$, $i = 1, 2, r, 4$, whose precise mathematical meanings are given in the appendix.

When $L \leq L_1(m)$,

$$L_1(m) = \sqrt{\frac{2-m}{m-1}}, \quad (26)$$

the situation is very similar to that for $m = 1$. A value of $R = R_r(L, m)$ exists (see figures 4 and 5) at which the axial velocity vanishes at the pipe wall, and

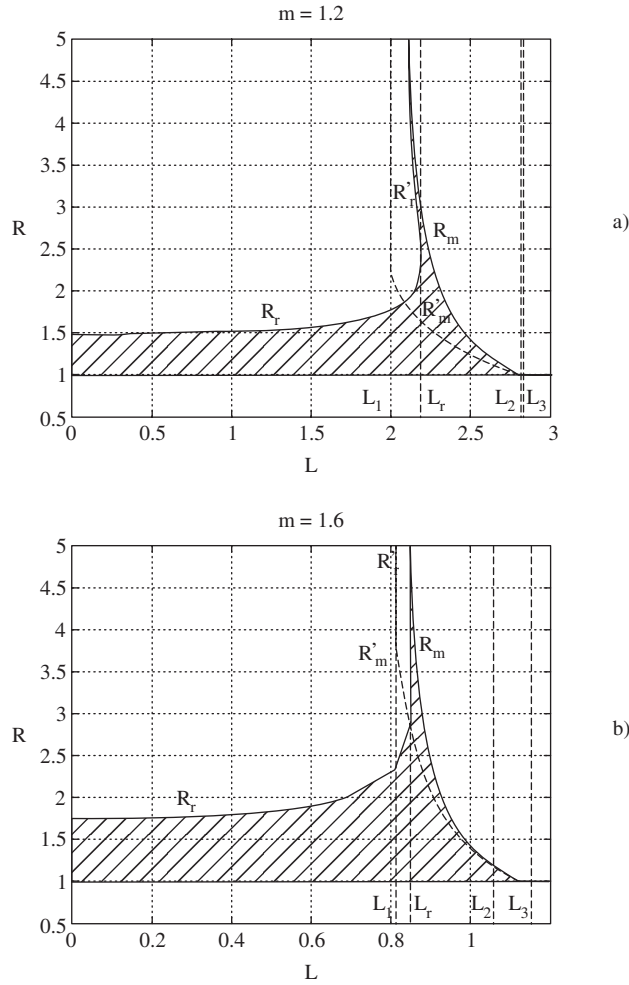


Figure 4. R_r , R'_r , R_m and R'_m as functions of L for $m = 1.2$ (a), and $m = 1.6$ (b). Dashed regions correspond to solutions with no cell of reversal flow near the wall.

above which a zone of flow reversal is formed near the wall (see figure 6 for several velocity profiles for $m = 1.2$ and different values of R). According to (16), R_r corresponds to $G(g) = -g$, which for $L \leq L_1$ has a single root $g = g_r = 2/(LR_r)^2$. One can see in figures 4 and 5 that R_r increases with m and L (remember that for $m = 1$ $R_r = \sqrt{2}$, independently of L). Thus, the introduction of swirl delays the onset of the near-wall zone of flow reversal: $R_r(L, m) \geq R_r(0, m)$ (R_r for $L = 0$ is depicted as a function of m in figure 7).

For $L_1(m) < L < L_r(m)$, where $L_r(m)$ is the folding value of $R_r(L)$ for each

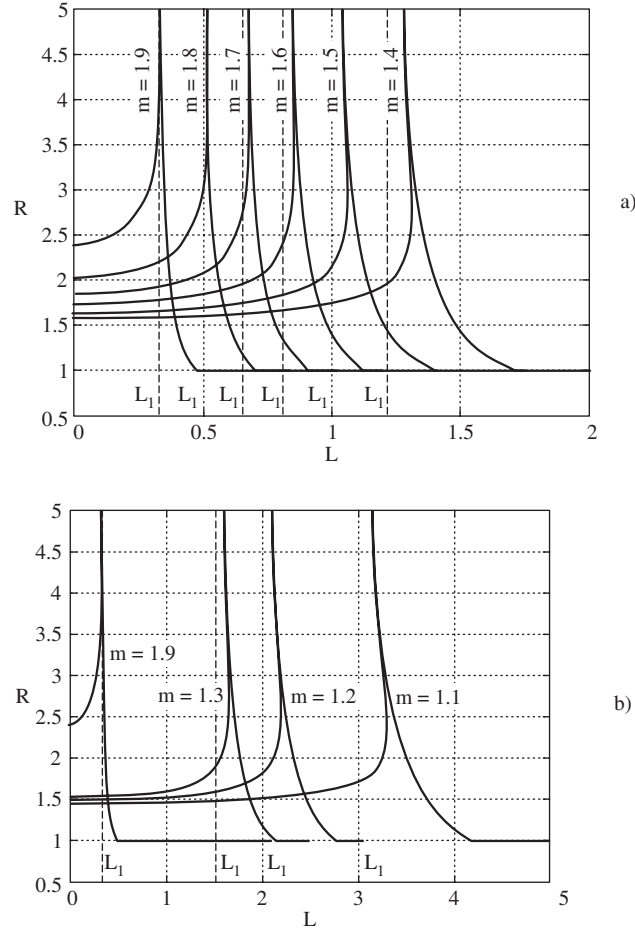


Figure 5.
 R_r , R_r' , and R_m as functions of L for several values of m in the range $1 \leq m < 2$.

m (see figure 4), and is obtained numerically and plotted in figure 3, several distinguished values of R exist separating different flow regimes (see figures 4-5). First, in addition to $R_r(m, L)$, a value $R_r'(m, L) > R_r$ exists above which the axial velocity at the wall becomes again positive, and the downstream flow presents *three cells* (R_r' is another root of $G(g) = -g$, see figure A2c in the appendix). That is, for a given value of L in the present range $L_1 < L < L_r$, as R increases above R_r , the downstream flow passes from a positive axial velocity everywhere to a two-cell flow with a near-wall backward velocity, and, when $R > R_r'$, a third near-wall cell is formed with positive axial velocity (see figure 6). However, R cannot increase much further because, as seen in figures 4 and 5, a maximum value $R_m(m, L)$,

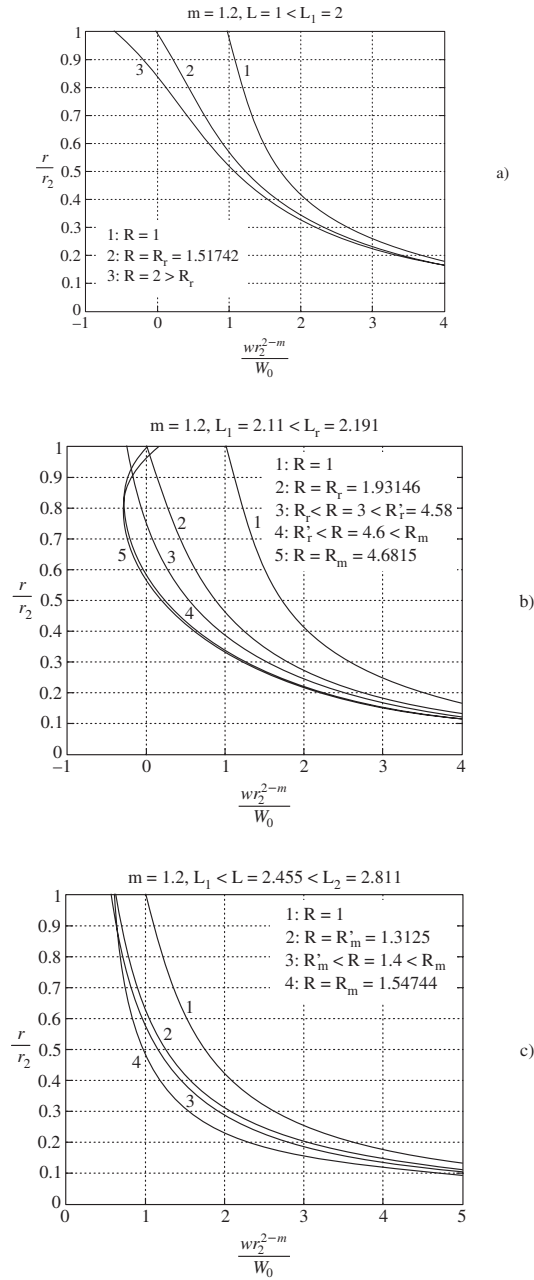


Figure 6. Dimensionless axial velocity profiles downstream for $m = 1.2$ and different values of R and L , as indicated.

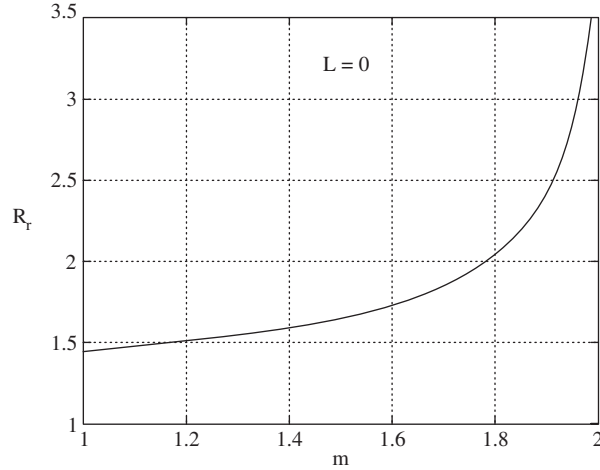


Figure 7.
 $R_r(m)$ for swirless ($L = 0$) flows.

slightly larger than R'_r , exists above which no solutions to the present problem are found. It must be noted that a value $R'_m(m, L) < R_m$ exists also (marked with a dotted line in figure 4) above which (i.e. for $R'_m < R < R_m$) several solutions satisfying the same boundary conditions may exist. However, as discussed above, only one of them, with or without zone of flow reversal, depending on whether R is smaller or larger than R'_r , is physically admissible.

Finally, in the range $L_r(m) \leq L < L_3(m)$, no zone of flow reversal appears for any radius R . The limiting value of R , R_m , is still present. The radius R'_m , above which a multiplicity of solutions for a given R exists, becomes equal to R_m for $L = L_2(m)$. Thus, for $L_2(m) \leq L \leq L_3(m)$, the region with multiplicity of solutions does not appear. When $L = L_3(m)$, $R_m = 1$, so that, as pointed out above, no solutions to the present problem for a diverging pipe exist when $L > L_3(m)$.

As discussed for the case $m = 1$, the solutions with reversal flow for $R > R_r$ (with $L < L_r$) are not unique because other boundary conditions for the backflow of the near-wall zone of flow reversal may be specified, which are not considered here. The particular solutions given here are for the same functions $H(\Psi)$ and $C(\Psi)$ of the inlet flow extended to the domain of the reversal flow from the outlet. Accordingly, for diverging pipes ($R > 1$), and for each value of m , the region on the (R, L) -plane where a unique solution to the present problem exists is below the curve $R_r(m)$ for $L < L_r(m)$, and below $R_m(m)$ for $L \geq L_r(m)$ (shaded areas in figure 4). For converging or straight pipes ($R \leq 1$), a unique solution exists for all the values of R and L .

We thus conclude that for the present inviscid models with singularity at the axis, inviscid breakdown either does not occur ($m = 1$), or the predicted values

of the swirl parameter for breakdown are, for the most interesting cases with m slightly larger than unity [7], far too larger than the observed ones (and predicted from the viscous axial boundary layer, i.e. $L^*(m)$ in figure 3).

4. Regularization of the inlet flow

Let's consider an inlet flow which is given by (5)-(6) for $r_c \leq r \leq r_1$, while for $0 \leq r \leq r_c$ the axial velocity is constant and the azimuthal velocity is linear with r (solid body rotation):

$$w = W_0 r_c^{m-2} \equiv W_1, \quad v = LW_1 \frac{r}{r_c}, \quad 0 \leq r \leq r_c; \quad (27)$$

$$w = W_1 \left(\frac{r}{r_c} \right)^{m-2}, \quad v = LW_1 \left(\frac{r}{r_c} \right)^{m-2}, \quad r_c \leq r \leq r_1. \quad (28)$$

For $m = 1$, the above azimuthal velocity corresponds to a Rankine vortex. This inlet flow for $m = 1$ is similar to that considered by Batchelor [2] modelling an isolated vortex (see also Stuart [14]), except in that we allow for a jet-like axial velocity with a radial potential decay, instead of assuming it uniform at the inlet. It must be noted that this *ad hoc* regularization at the axis of the inlet inviscid flow (28) by a central core of the form (27) leads, of course, to w and v profiles different to those brought about by viscous effects near the axis (see [7]), where an inviscid formulation is questionable. However, (27)-(28) has some of the main features of a real swirling jet, and is a valid solution of the *cylindrical* Euler equations, like any velocity profile of the form $(0, w(r), v(r))$. It is thus worth pursuing its evolution through the B-H equation, as previously done for different inlet flows by Batchelor [2], and by Buntine and Saffman [5], among others.

For $0 \leq r \leq r_c$,

$$\Psi = W_1 \frac{r^2}{2}. \quad (29)$$

Hence, the functions $C(\Psi)$ and $H(\Psi)$ are given by

$$C = vr = \frac{2L}{r_c} \Psi, \quad H = \frac{1}{2} w^2 + \int^r \frac{C}{r^2} \frac{dC}{dr} dr = \frac{1}{2} W_1^2 + \frac{2L^2 W_1}{r_c^2} \Psi, \quad (30)$$

for $0 \leq \Psi \leq W_1 r_c^2 / 2$. Equation (4) becomes

$$\Psi_{rr}^{(i)} - \frac{1}{r} \Psi_r^{(i)} = \frac{2L^2}{r_c^2} (W_1 r^2 - 2\Psi^{(i)}) \quad (0 \leq \Psi^{(i)} \leq W_1 r_c^2 / 2), \quad (31)$$

where the superscript (i) stands for the *inner* flow inside the core. The general solution of this equation is of the form [2]

$$\Psi^{(i)} = \frac{1}{2} W_1 r^2 + Ar J_1(kr) + Br Y_1(kr), \quad (32)$$

where A and B are arbitrary constants, J_1 and Y_1 are first order Bessel functions of the first and second kind, and

$$k = \frac{2L}{r_c}. \quad (33)$$

The boundary condition at the axis sets $B = 0$. Constant A will be determined by the matching with the outer solution at the downstream vortex radius r_b , which is also unknown (see below).

For $r_c < r < r_1$, according to (27)-(28),

$$\Psi = \frac{W_1 r_c^2}{m} \left[\left(\frac{r}{r_c} \right)^m + \frac{m-2}{2} \right], \quad (34)$$

so that

$$C(\Psi) = LW_1 r_c \left(\frac{m\Psi}{W_1 r_c^2} + \frac{2-m}{2} \right)^{(m-1)/m}, \quad (35)$$

and

$$H(\Psi) = \frac{m-3}{2(m-2)} (LW_1)^2 + \frac{W_1^2}{2} \left(1 - \frac{m-1}{2-m} L^2 \right) \left(\frac{m}{W_1 r_c^2} \Psi + \frac{2-m}{2} \right)^{2(m-2)/m}, \quad (36)$$

valid for

$$\frac{1}{2} W_1 r_c^2 \leq \Psi \leq \frac{W_1 r_c^2}{m} \left[\left(\frac{r_1}{r_c} \right)^m - \frac{2-m}{2} \right]. \quad (37)$$

Using the dimensionless variables

$$y = \frac{1}{2} \left(\frac{r}{r_c} \right)^2, \quad \psi^{(o)} = \frac{m}{W_1 r_c^2} \Psi^{(o)} + \frac{2-m}{2}, \quad (38)$$

where the superscript (o) is for *outer* flow, the B-H equation in this region becomes

$$\psi_{yy}^{(o)} = m(2-m) \left(\frac{m-1}{2-m} L^2 - 1 \right) \psi^{(o)1-4/m} - \frac{L^2 m(m-1)}{2y} \psi^{(o)1-2/m}. \quad (39)$$

Obviously, this equation has the same form as (9). The boundary conditions are, however, quite different:

$$\Psi^{(o)}(r_b) = \Psi^{(i)}(r_b) = \frac{1}{2} W_1 r_c^2, \quad (40)$$

$$\frac{d}{dr} \Psi^{(o)}(r_b) = \frac{d}{dr} \Psi^{(i)}(r_b), \quad (41)$$

$$\Psi^{(o)}(r_2) = \frac{W_1 r_c^2}{m} \left[\left(\frac{r_1}{r_c} \right)^m + \frac{m-2}{2} \right]. \quad (42)$$

The first two conditions state that at the outlet core radius r_b the inner and outer stream functions and their derivatives (axial velocities) are continuous, and that the stream function takes the inlet value for $r = r_c$. Condition (42) assures that the pipe wall is a streamline. Equations (40)-(42) constitute a set of four conditions to fix r_b , the integration constant A in (32), and the two integration constants resulting from (39). The cases $m = 1$ and $m \neq 1$ are considered separately next. To check these cylindrical solutions, they are compared with numerical results from the non-cylindrical B-H equation for $m = 1$ and the particular pipe form (24).

4.1. $m = 1$

Equation (39) has an analytic general solution in this case, and the four conditions (40)-(42) become a relatively simple set of algebraic equations. (Equation (39) may be written in the form (14), whose phase plane is analysed in the appendix. However, we shall not use that form of the equation for $m = 1$, but in the numerical integration for the cases $1 < m < 2$; see next section.)

Putting $m = 1$ in (39), one obtains

$$\psi_{yy}^{(o)} = -\psi^{(o)-3}, \quad (43)$$

which has the general solution

$$\psi^{(o)} = \sqrt{(y+E)^2/D - D}, \quad (44)$$

with D and E arbitrary constants. Equations (40)-(42) yield the following four relations:

$$1 = b^2 + abJ_1(2Lb), \quad (45)$$

$$b^2/2 + E = \sqrt{D(D+1)}, \quad (46)$$

$$1 + aLJ_0(2Lb) = \sqrt{1 + \frac{1}{D}} \quad (47)$$

$$R_2^2/2 + E = \sqrt{D(D+R_1^2)}, \quad (48)$$

where

$$R_1 = \frac{r_1}{r_c}, \quad R_2 = \frac{r_2}{r_c}, \quad a = \frac{2A}{W_1 r_c}, \quad \text{and } b = \frac{r_b}{r_c}, \quad (49)$$

are, like D and E , dimensionless parameters. Eliminating a and E , one has the following set of two non-linear algebraic equations to obtain the dimensionless

outlet core radius b (and parameter D) as a function of the dimensionless inlet and outlet pipe radii, R_1 and R_2 , and the swirl parameter L :

$$\frac{R_2^4 - b^4}{4} + D \left[1 + R_2^2 \sqrt{1 + \frac{1}{D}} - R_1^2 - b^2 \sqrt{1 + \frac{R_1^2}{D}} \right] = 0, \quad (50)$$

$$b^2 - 1 + \left(\sqrt{1 + \frac{1}{D}} - 1 \right) \frac{bJ_1(2Lb)}{LJ_o(2Lb)} = 0. \quad (51)$$

Figures 8 and 9 show the outlet core radius b as a function of the swirl parameter L for several values of R_1 and R_2 . Also shown in these figures is the outlet dimensionless axial velocity at the axis,

$$\xi \equiv \frac{w(r=0)}{W_1} = 1 + aL = 1 + \left(\sqrt{1 + \frac{1}{D}} - 1 \right) \frac{1}{J_o(2Lb)}. \quad (52)$$

For comparison, we have included in figure 9 the corresponding values of b and ξ given by Batchelor's solution [2] for an "isolated" vortex (dotted lines), which corresponds to the present problem with $m = 1$ when there is no radial decay of the axial velocity outside the vortex core. That is, at the pipe inlet $w = W_1$ everywhere, and at the outlet $w = W_2 = \text{constant}$ for $r > r_b$, where, by continuity,

$$\frac{W_2}{W_1} = \frac{R_1^2 - 1}{R_2^2 - b^2}. \quad (53)$$

Substituting this expression into Batchelor's solution in terms of W_2/W_1 , one obtains the following relations for b and ξ :

$$b^2 - 1 + \left(\frac{R_1^2 - 1}{R_2^2 - b^2} - 1 \right) \frac{bJ_1(2Lb)}{LJ_o(2Lb)} = 0, \quad (54)$$

$$\xi = 1 + \left(\frac{R_1^2 - 1}{R_2^2 - b^2} - 1 \right) \frac{1}{J_o(2Lb)}. \quad (55)$$

The main feature of the functions $b(L)$ and $\xi(L)$ given in figures 8 and 9 is that, for diverging pipes ($R_1 < R_2$), there exists a folding value of the swirl parameter, L_f , which depends on R_1 and R_2 , above which no solution exists, while a solution always exists for any value of L in a converging pipe ($R_1 > R_2$). Therefore, the quasi-cylindrical approximation fails above a critical value of L for a diverging pipe. When this occurs, the numerical solution to the non-cylindrical B-H equation shows a "bubble" form of vortex breakdown downstream (see figure 10). Another important feature observed in the figures 8 and 9 is that, also for $R_1 < R_2$, a stagnation point ($\xi = 0$) is reached at the axis for a value $L_o < L_f$. Thus, for

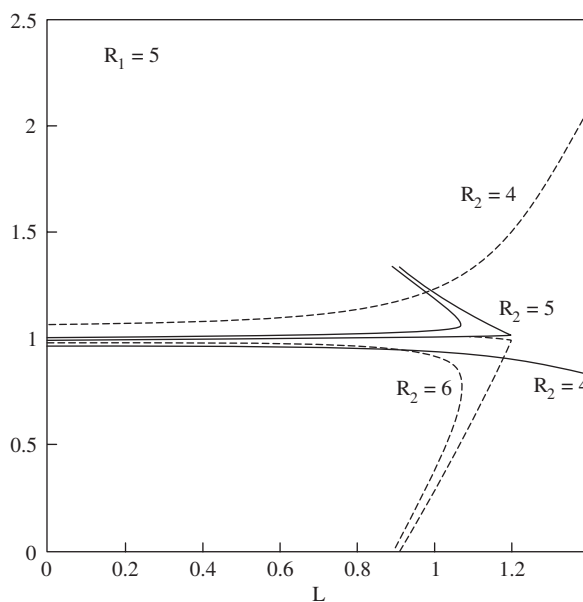


Figure 8.
Functions $b(L)$ (continuous lines) and $\xi(L)$ (dashed lines) for $m = 1$, and for $R_1=5$, with $R_2 = 4, 5, 1$ and 6 .

$L_o < L < L_f$, two different solutions exist for the same value of the swirl parameter in a diverging pipe. They correspond to two of the three different solutions found by Wang and Rusak [6] for $L_o < L < L_f$ in the case of a straight pipe. (The third solution with a stagnant, or flow reversal, region near the axis, valid for $L > L_o$, is not looked for in the present formulation. Keller et al. [3] found that, in order to obtain this type of cylindrical solution with an axial stagnant zone, the additional condition of flow force conservation has to be imposed on the solution.) As a matter of fact, for a straight pipe ($R_1 = R_2$ or $R = 1$), although a folding value of L is not found (the inlet solution, $b = \xi = 1$, is valid for any swirl number), the second solution given by Wang and Rusak is also found in the present quasi-cylindrical formulation for $L > L_o$, crossing the first (inlet) solution for a value L_{fm} given by $J_o(2L_{fm}) = 0$ ($L_{fm} \simeq 1.2$). L_{fm} thus constitutes a maximum or limiting value for the folding swirl number L_f as R_1 and $R_2 > R_1$ vary (see figure 11 in addition to figure 9). It coincides with the critical swirl of Benjamin [1].

These general features are also observed for Batchelor's inlet model [2]. Actually, for a straight pipe ($R = 1$) both sets of solutions are very similar: One has the inlet solution ($b = \xi = 1$) crossed by a second solution at $L = L_{fm}$. In the case of Batchelor's inlet flow, these two solutions are easily obtained putting $R_1 = R_2$ in (54)-(55):

$$b_1 = \xi_1 = 1, \quad (R = 1), \quad (56)$$

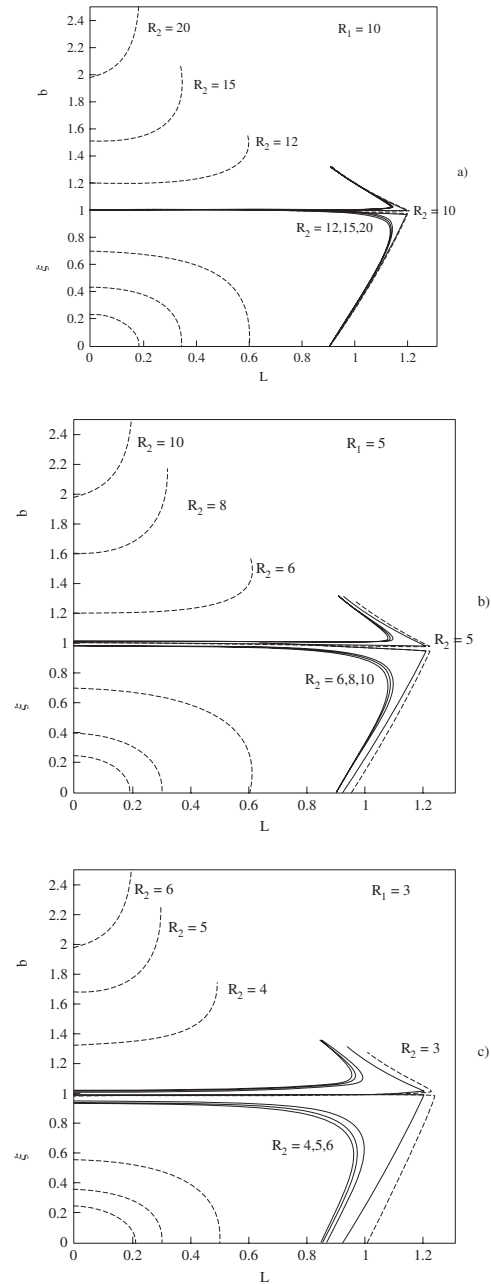


Figure 9. Functions $b(L)$ and $\xi(L)$ given by (50)-(52) for $m = 1$ (continuous lines), and obtained from Batchelor's model (54)-(55) (dotted lines) for several values of R_1 and $R_2 > R_1$: (a) $R_1 = 10$ and $R_2 = 20, 15, 12, 10.0001$; (b) $R_1 = 5$ with $R_2 = 10, 7, 6, 5.0001$, and (c) $R_1 = 3$ with $R_2 = 6, 5, 4, 3.0001$.

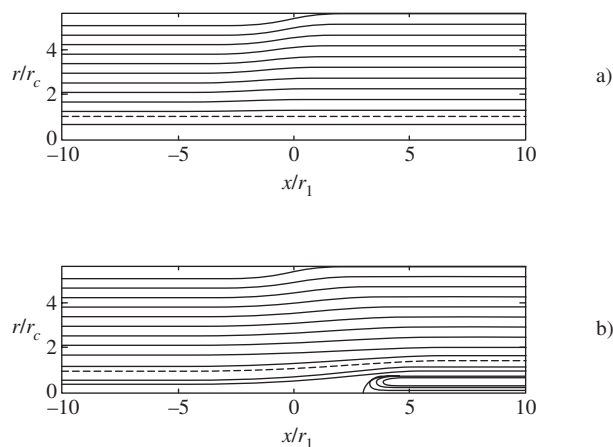


Figure 10.

Streamlines obtained numerically from the non-cylindrical B-H equation (2) with the pipe geometry (24), using the regularised inlet velocity (27) and (28) with $m = 1$, $R_1 = 5$ and $R = 1.1$, for $L = 0.5$ (a) and $L = 1.23 > L_f \simeq 1.05$ (b). The dashed streamlines correspond to the core radius.

and

$$(R_1^2 - b_2^2)LJ_o(2Lb_2) + b_2J_1(2Lb_2) = 0, \quad \xi_2 = 1 - \frac{(b_2^2 - 1)L}{b_2J_1(2Lb_2)}, \quad (R = 1), \quad (57)$$

which are also depicted in figure 9. However, as R_2 becomes larger than R_1 , the values of L_o and L_f obtained with Batchelor's constant axial inlet velocity are much more strongly dependent on the pipe radii, R_1 and R_2 , than those obtained with the present inlet flows. Thus, by just allowing for a radial decay of the axial velocity, L_f becomes less dependent on R_1 and R_2 , ranging typically between 1 and 1.2 in the present model, more in agreement with many experimental and numerical results on vortex breakdown (e.g. Spall, Gatski and Grosch [15], Beran and Culik [9]). Similar results were obtained by Buntine and Saffman [5] using an exponential decay for both the axial and the azimuthal inlet velocity outside the vortex core. This is more clearly seen in figure 11, where L_f and L_o are plotted as a function of $R \geq 1$ for both inlet flows models, and for two values of R_1 . With the present inlet model flow for $m = 1$, L_f remains between 1.05 and 1.2, approximately, with $L_f \rightarrow L_{fm} \simeq 1.2$ as $R \rightarrow 1$. The stagnation value L_o remains almost constant ($L_o \simeq 0.9$) as R increases. On the other hand, using a constant inlet axial velocity, the resulting L_o and L_f decay rapidly as R increases. For sufficiently large values of R , the folding value of L may even disappear using Batchelor's inlet flow (see figure 9; this value of R depends on R_1 , but one can see in figure 11 that it typically lies between $R = 1.2$ and $R = 1.4$). In these cases, a *mild* transition to a stagnation point at the axis without folding is produced

when the value of L_o is reached. Thus, the hysteresis topology of the inviscid breakdown given by Wang and Rusak [6] does not exist for these cases, and the solution with stagnation at the axis may be reached without an abrupt transition. A similar situation with no fold for sufficiently large pipe divergence has been recently reported by Rusak, Judd and Wang [16]. These authors analysed the effect of small pipe divergence on near critical swirling flows finding asymptotically that, in our notation, $L_{fm} - L \simeq \alpha\sqrt{R-1}$ when $R-1$ is small, where α is a constant depending on the pipe geometry and on the inlet flow considered. This is in agreement with our results for $0 < R-1 \ll 1$ (see figure 11; for Batchelor's inlet flow we find $\alpha \simeq 1.4$, which is almost independent of R_1 , while for the present inlet model flow with $m = 1$, α is smaller and depends on R_1).

It is interesting to analyse asymptotically the case of R_1 and R_2 large, because it corresponds to the slender cores typical of high Reynolds numbers flows, for which the present inviscid picture would make most sense. From equations (50)-(52), the first solution branches of $b(L)$ and $\xi(L)$ are unity in first approximation, and the next corrections are given by ($R_1 \gg 1$):

$$\begin{aligned} b_1 &= 1 + \frac{1}{R_1^2} \frac{J_1(2L)}{LJ_o(2L)} \frac{R^2 - 1}{R^4} + O(R_1^{-4}) \\ \xi_1 &= 1 - \frac{1}{R_1^2} \frac{2}{J_o(L)} \frac{R^2 - 1}{R^4} + O(R_1^{-4}) \text{ for } R \equiv \frac{R_2}{R_1} \neq 1, \end{aligned} \quad (58)$$

and

$$b_1 = \xi_1 = 1 \text{ for } R = 1, \quad (59)$$

so that for a straight pipe the core radius remains also unchanged. The second solution branch can be written in a simpler form than (50)-(52) for a straight pipe, but not for $R \neq 1$. In first approximation b_2 and ξ_2 are given by

$$LJ_o(2Lb_2) + \frac{2}{R_1^2} b_2 J_1(2Lb_2) = 0, \quad \xi_2 = 1 + \frac{(1 - b_2^2)L}{b_2 J_1(2Lb_2)} \text{ for } R = 1. \quad (60)$$

For Batchelor's inlet model, the first branches of b and ξ are not unity at the lowest order for $R \neq 1$ (see for instance figure 9a), but given by

$$b_1^2 - 1 + \frac{1 - R^2}{R^2} b_1 \frac{J_1(2Lb_1)}{LJ_o(2Lb_1)} = 0, \quad \xi_1 = 1 + \frac{1 - R^2}{R^2} \frac{1}{J_o(2Lb_1)}, \quad R \neq 1. \quad (61)$$

For $R = 1$, $b_1 = \xi_1 = 1$, as in the model considered in the present paper. The second branch is different from (60), and given, at the lowest order, by

$$LJ_o(2Lb_2) + \frac{1}{R_1^2} b_2 J_1(2Lb_2) = 0, \quad \xi_2 = 1 - \frac{L}{b_2 J_1(2Lb_2)}, \quad R = 1. \quad (62)$$

4.2. Results for $1 < m < 2$

For $m \neq 1$, one has to solve numerically equation (39) with boundary conditions (40)-(42) in order to obtain $b(L)$ for different values of m , R_1 and R_2 . To this end, it is more convenient to use that equation written in the form (13)-(14), using $m\psi^{(o)}/W_o$ instead of Ψ in the definition (12) of g , and replacing η by y , which just turns formally (13) into $dg/dy = G/y$, and leaves (14) unchanged. Written in this form, one may take advantage of the phase plane structure analysed exhaustively in the appendix to perform the numerical integration. However, many of the phase-plane subtleties discussed in the appendix are irrelevant here because the axis of the pipe is now out of the range of application of equation (14), and because, from the analysis given in the preceding section, we are mostly interested in values of R slightly larger than, or equal to, unity.

The boundary condition (42) at the wall becomes

$$g = \frac{2}{(LR)^2}, \text{ for } y = \frac{1}{2}R_2^2. \quad (63)$$

The boundary condition at the radius of the core, (40)-(41), substituting the inner solution (32) and eliminating constant A , may be written as

$$g = \frac{2}{(Lb)^2} \text{ and } G = \frac{2}{L^2} \left(1 + \frac{1-b^2}{b} L \frac{J_o(2Lb)}{J_1(2Lb)} - \frac{1}{b^2} \right) \text{ for } y = \frac{1}{2}b^2. \quad (64)$$

To solve this problem one may proceed by shooting. An efficient way to do so is to assume a value of b , for each value of m , L , R_1 and R_2 , and obtain from (64) g and G at the core radius. From these values start the numerical integration towards the pipe radius, and change there the guessed value of b until both g and y are given by (63) simultaneously.

Figure 12 shows $b(L)$ and $\xi(L)$ for different values of m , R_1 , and R_2 (for diverging pipes; $R_2 > R_1$), comparing these functions with the corresponding ones for $m = 1$ of figure 9. The main feature observed in the figure is that both the folding and stagnation values of L , L_f and L_o , decrease as m increases from unity. This is shown more clearly in figure 13, where $L_f(m)$ and $L_o(m)$ are plotted for different values of R_1 and R_2 . L_f approaches L_o as m increases from unity, but a folding value $L_f > L_o$ always exists, except for straight pipes ($R_2 \rightarrow R_1$) above a relatively large value of m (remember that, physically, the most interesting values of m are those near unity). Also included in this figure is $L^*(m)$ from [7].

5. Concluding remarks

Using two simple models for the inlet swirling flow in a pipe we have shown that the inviscid equations predicts vortex breakdown only for inlet profiles regular at

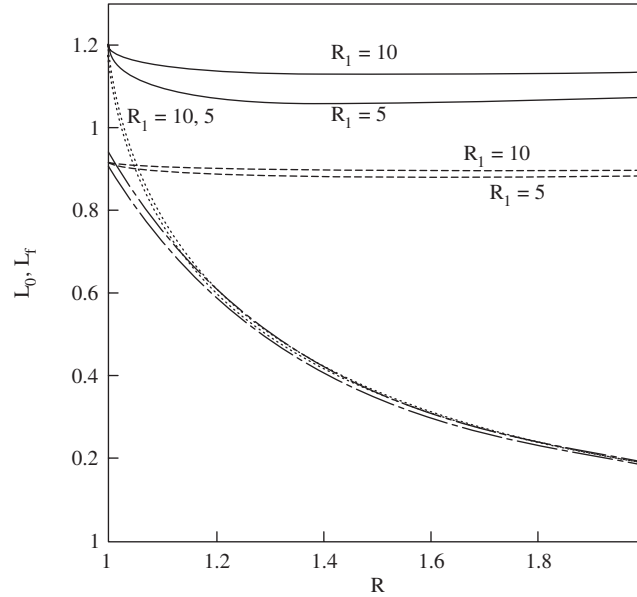


Figure 11.

L_f (continuous lines) and L_o (dashed lines) as functions of R for $R_1 = 5$ and 10 ($m = 1$). Dotted, and dotted and dashed, lines correspond to Batchelor's inlet model.

the axis. Hence it is argued that the presence of viscosity, which is the agent regularising the usually singular behaviour at the axis of inviscid swirling flows (e.g. [8],[7]), is essential for vortex breakdown to occur in pipes. Of course, the simple exercise here presented is far from conclusive on the question about the importance of viscosity on vortex breakdown, but we believe that it adds some new elements to it. To settle the problem (at least in pipes), one has to carry out numerical simulations of swirling flows in pipes using the full viscous equations, but with more realistic inlet boundary conditions far upstream than the previously used by some investigators, and compare them with both rigorous inviscid simulations and experiments. As found by Darmofal in his recent Navier-Stokes numerical simulations of the swirling flow in a pipe [11], the breakdown location was "extremely sensitive to small variations in inlet conditions", which were adjusted from experimental measurements, whence the importance of the precision in the inlet boundary conditions. It may be argued that if the presence of viscosity is essential for vortex breakdown to occur, why the inviscid simulations (but with viscosity *hidden* in the inlet flow) predict so reasonably well breakdown? The answer may be that, even if the absence of axial singularity (or the presence of viscosity) is essential for vortex breakdown, the parameter governing it, the swirl number, is purely inviscid, and so the mechanism producing breakdown is mostly inviscid, as shown by many previous works on the subject (e.g. [1]-[6],[14]). As noted earlier

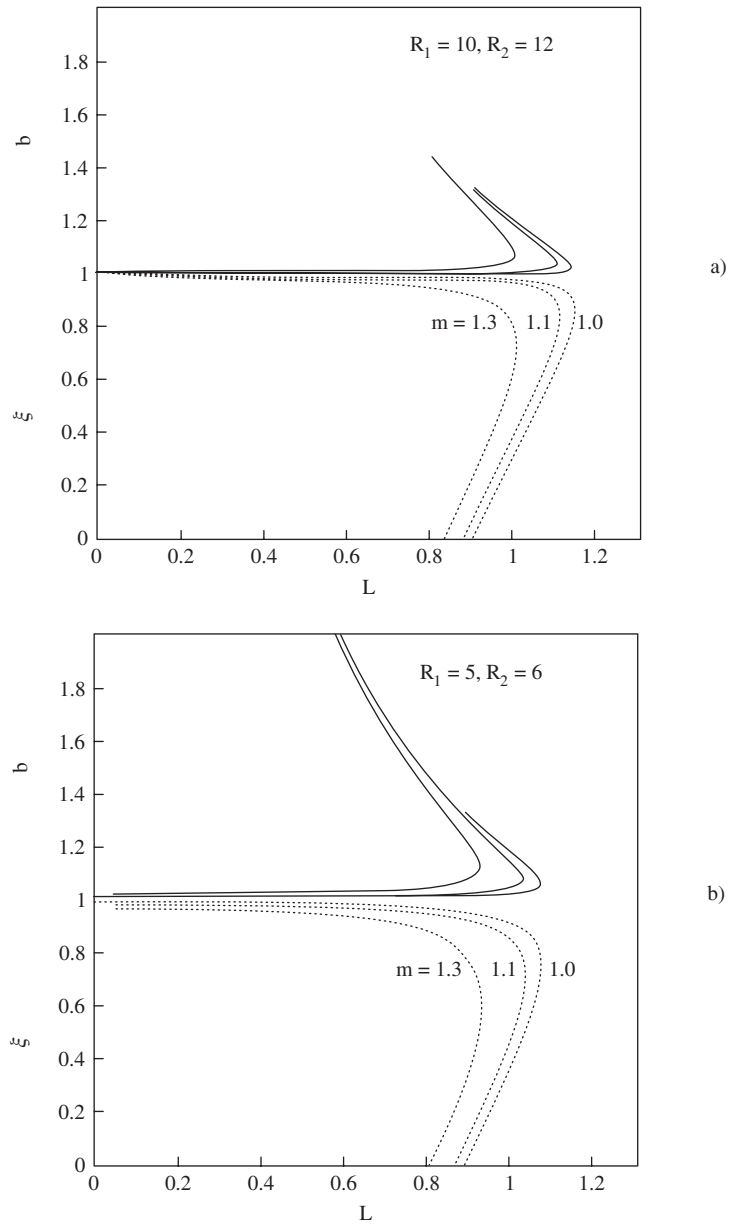


Figure 12.
 $b(L)$ (continuous lines) and $\xi(L)$ (dotted lines) for different values of m , R_1 and R_2 , as indicated.

by Hall [12], Beran and Culik [9], and others, something similar happens in the

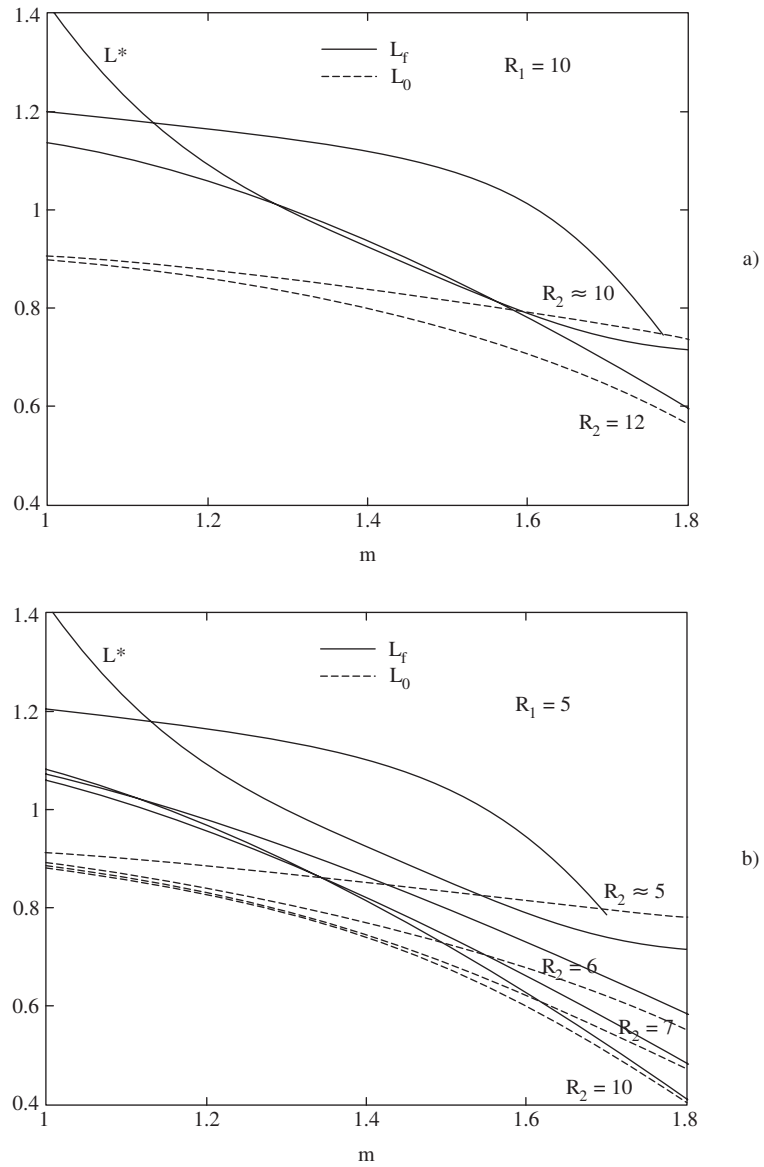


Figure 13.

$L_f(m)$ (continuous lines) and $L_o(m)$ (dotted lines) for $R_1 = 10$ (a) and $R_1 = 5$ (b), and for several values of R_2 . Also included is $L^*(m)$.

phenomenon of boundary layer separation: although without viscosity there is no separation, it is produced by adverse pressure gradients, therefore controlled by

external inviscid factors, and predicted by inviscid arguments. From the present and previous cited results it may be inferred that the details of how viscosity actually regularises the inviscid flow at the axis are less important for the (qualitative) prediction of breakdown than the fact that viscosity is taken into account in the inlet velocity profile in a more or less crude form. In other words, viscosity is indirectly (and trivially) essential in vortex breakdown in generating a regular vortex flow.

Independently of the viscosity question, the inviscid models here presented show that it is important to take into account the radial decay of the inlet axial flow in order to correctly predict the critical swirl number above which *inviscid* vortex breakdown occurs. If one assumes an uniform axial velocity [2], the critical swirl number is much more dependent on the outlet radius of the pipe than the observed values, being appreciably smaller. Using a potential radial decay we have shown, as previously Buntine and Saffman [5] using an exponential decay, that the inviscidly predicted critical swirl numbers are almost independent of the outlet radius, in accordance with experiments.

Acknowledgements

This work owes very much to Professor Fernandez de la Mora (Yale University), with whom one of the authors (RFF) has discussed it at large thanks to a NATO Collaborative Research Grant, CRG 950368. It has also been supported by the Dirección General de Investigación Científica y Técnica of Spain, Grants PB93-0974 and PB96-0679.

Appendix: Phase plane structure of (14)

In addition to be essential for the numerical integrations behind the results given in sections 3.2 and 4.2, the present phase plane analysis of equation (14) helps showing the different regimes present in the flow as the three dimensionless parameters of the problem of section 3, L , R and m , vary.

Let's consider first the case $m = 1$. Equation (19) has four singular points: two saddle points, $(G = 0, g = \pm 2/L^2)$, and two degenerate nodes, $(G = \pm 2/L^2, g = 0)$. The trajectories going through these singular points are the four straight lines (see figure A1)

$$G = \pm \left(g \pm \frac{2}{L^2} \right). \quad (65)$$

The saddle point $(G = 0, g = 2/L^2)$ corresponds to the axis of the pipe. Indeed, the boundary condition at the axis (11a) implies from (9) $\Psi = Ar$ (i.e., the same kind of upstream singularity of the axial velocity at the axis is preserved downstream), where $A = (\pm 1)^{1/2} W_0$. The two possible solutions correspond, respectively, to

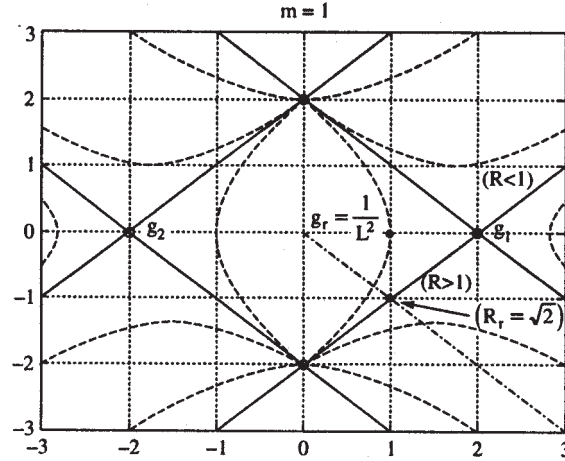


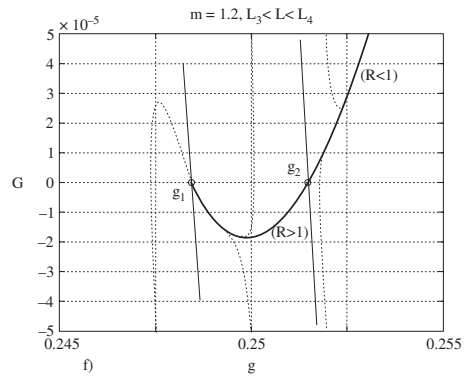
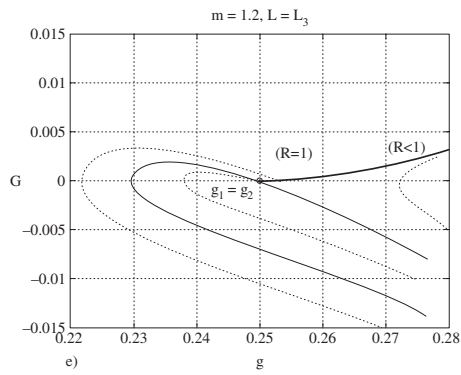
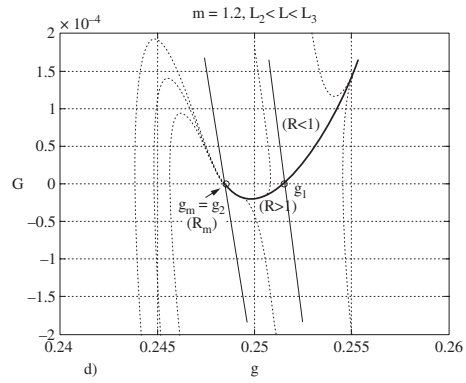
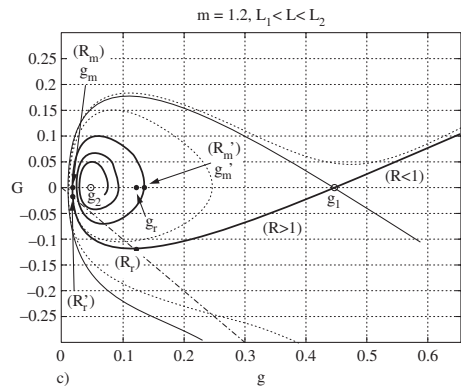
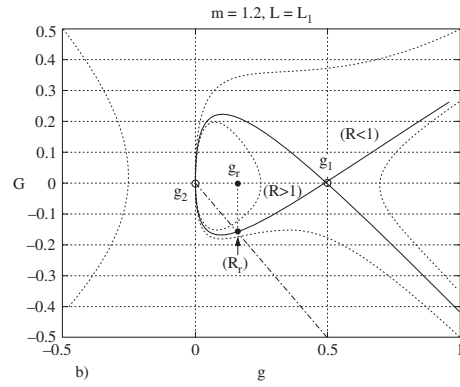
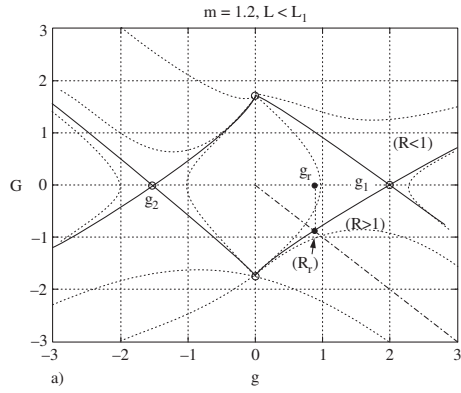
Figure A1.
Phase plane (G vs. g) for $m = 1$.

the singular points ($G = 0, g = \pm 2/L^2$), of which, obviously, that corresponding to the minus sign must be discarded. Since, according to (65) and (12)-(13), the solution near the point ($G = 0, g = 2/L^2$) behaves as

$$\Psi = W_0 r (1 + c\eta^{\pm 1})^{1/2} \quad (66)$$

in physical variables, where c is a positive arbitrary constant to be determined by the wall boundary condition (see (22)), and the \pm sign correspond, respectively, to the \pm sign of the slope in the straight lines (65), the only trajectory of physical interest in the present problem is that with positive slope going through this saddle point; i.e. $G = g - 2/L^2$.

The pipe wall is reached when $g = 2/(LR)^2$, so that a converging pipe ($R < 1$) is described by the half trajectory going upwards from the saddle point ($G > 0$ or $g > 2/L^2$, see figure A1), the singular point itself corresponding to a straight pipe ($R = 1$), and a diverging pipe ($R > 1$) to the trajectory going downwards from the saddle point towards the node ($G = -2/L^2, g = 0$). This last point corresponds to the wall of a pipe with a downstream infinite radius. But, before reaching this point, a zone of reversal flow appears near the wall when $R > \sqrt{2}$. Indeed, for $R = \sqrt{2}$, corresponding to the crossing point between the trajectory $G = g - 2/L^2$ and the bisector $G = -g$ ($g = -G = 1/L^2$), the axial velocity, which is proportional to $G + g$ (see (16)), vanishes at the wall. In the case of a converging pipe, this zone of reversal flow is never formed for any value of R , and a pipe with vanishing radius downstream corresponds to $g \rightarrow \infty$ along the trajectory $G = g - 2/L^2$.



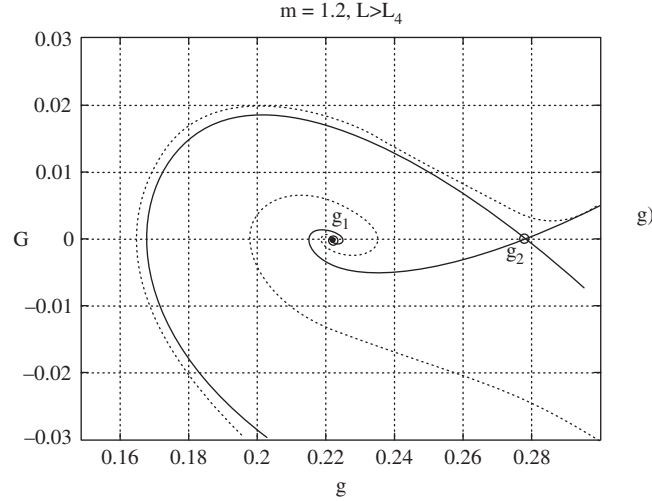


Figure A2.

Phase plane for $m = 1.2$. (a): $L < L_1$ ($L = 1$). (b): $L = L_1 = 2$. (c): L between L_1 and L_2 ($L = 2.5$; $L_2 \simeq 2.811$). (d): L between L_2 and L_3 ($L = 2.8198$; $L_3 \simeq 2.828$). (e): $L = L_3$. (f): L between L_3 and L_4 ($L = 2.8372$; $L_4 \simeq 2.846$). (g): $L > L_4$ ($L = 3$).

The different phase plane structures for $1 < m < 2$ as L increases are depicted in figure A2 for the particular value $m = 1.2$. When $L < L_1(m)$, the structure is very similar to that for $m = 1$ (fig. A2a), where

$$L_1(m) = \sqrt{\frac{2-m}{m-1}} \quad (67)$$

(plotted in figure 3). In this case there are four singular points: two saddle points,

$$(G = 0, g = g_1) \text{ and } (G = 0, g = g_2), \quad g_1 = \frac{2}{L^2}, \quad g_2 = \frac{2(m-1)}{2-m} - \frac{2}{L^2}, \quad (68)$$

and two nodes, $(G = G_{\pm}, g = 0)$, where

$$G_{\pm} = \pm \frac{2}{L^2} \left[1 - \frac{(m-1)L^2}{2-m} \right]^{1/2}.$$

As in the case $m = 1$, the saddle point $(G = 0, g = g_1 = 2/L^2)$ corresponds to the axis of the pipe: According to (9), the vanishing stream function near the axis should behave as $\Psi = (W_o L^m / m)(g_i \eta)^{m/2}$ (again, the singularity of the axial velocity is preserved along the axis), where the g_i , $i = 1, 2$, are given by (68). Since $g_2 < 0$ for $L < L_1$, the solution corresponding to the other saddle point, $(G = 0, g = g_2)$, has no meaning in physical variables. On the other hand, since the

behaviour near the saddle point ($G = 0, g = 2/L^2$) is given, in physical variables, by (compare with (66))

$$\Psi = \frac{W_o}{m} r^m (1 + c\eta^{a_{1\pm}})^{m/2}, \quad (69)$$

where $a_{1\pm}$, $a_{1+}a_{1-} < 0$, are the two roots of

$$a_1^2 - (1 - m)a_1 - 2 + m - (1 - m)/g_1 = 0, \quad (70)$$

which also correspond to the two slopes of the two trajectories crossing that singular point,

$$G = a_{1\pm}(g - g_1),$$

it follows that, as in the case $m = 1$, only the trajectories with positive slope are of physical interest. For a converging pipe ($R < 1$), the downstream solution is given by the trajectory going upwards (see figure A2a), the point at infinity corresponding to a pipe with vanishing downstream radius. For a diverging pipe ($R > 1$), the solution is that going downwards towards the nodal point ($G = G_-, g = 0$), which corresponds to $R \rightarrow \infty$. But, before reaching this point, when the trajectory crosses the bisector $G = -g$ at $g = g_r(m, L)$, corresponding to a dimensionless pipe radius $R = R_r(L, m) = \sqrt{(2/g_r)}/L$ (remember that $R_r = \sqrt{2}$ for $m = 1$ and for any L), the axial velocity vanishes at the pipe wall and a cell with flow reversal is formed near the wall for $R > R_r$ (see figure 2, and figure 6a).

When $L = L_1$, the two nodal points merge into the origin, together with the saddle point that was on the negative g -axis for $L < L_1$ (see figure A2b). The physically meaningful solution is, however, very similar to that for $L < L_1$. When $L > L_1$, the two singular points lying on the G -axis have disappeared, and the one on the negative g -axis has passed to the positive side, so that only the two singular points (68) remain, both on the positive side of the g -axis (g_1 and g_2 are now positive). While $L < L_3(m)$, where

$$L_3 = \sqrt{2}L_1 = \sqrt{\frac{2(2-m)}{(m-1)}} \quad (71)$$

(plotted in figure 3), $g_1 = 2/L^2$ is larger than g_2 , and the right singular point ($G = 0, g = g_1$) remains a saddle point, which corresponds to the axis of the tube. However, the left singular point ($G = 0, g = g_2$) is no longer a saddle, but a stable spiral when $L_1 < L < L_2(m)$, where

$$L_2 = \frac{3-m}{\sqrt{m^2-4m+5}} L_1, \quad (72)$$

(see figure A2c for $m = 1.2$ and $L = 2.5$; $L_2(m)$ is plotted in figure 3), and a stable nodal point for $L_2 \leq L < L_3$ (figure A2d, for $m = 1.2$ and $L = 2.8198$; note

that, for $m = 1.2$, $L_2 \simeq 2.811$ and $L_3 \simeq 2.828$). Since (69)-(70) are still valid, the trajectory of physical interest is always the separatrix crossing the saddle point ($G = 0, g = 2/L^2$) with positive slope. For a converging pipe ($R < 1$) the situation is the same as described above. However, for a diverging pipe ($R > 1$), and when $L_1 < L < L_2$, the bisector $G = -g$ may cross the separatrix in two points, be tangent to it, or not cross it at all. In the first case, which occurs for $L_1 < L < L_r(m)$, where $L_r(m)$ is plotted in figure 3, two critical radii $R_r(m)$ and $R'_r(m, L) > R_r$ exist corresponding to the crossing points g_r and g'_r of the bisector with the physical trajectory (figure A2c). When $R > R'_r$, another cell is formed in the flow near the wall, where the axial velocity is again positive (see figure 6b). In the other two cases, taking place for $L_r \leq L < L_2$, no zone of flow reversal is produced for any value of R . This is not, however, the most important difference in a diverging pipe for $L_1 < L < L_3$ in relation to the previous cases, but the existence of another critical value of R , $R_m(m, L)$, corresponding to the crossing of that separatrix with the g -axis, $g = g_m(m, L)$ ($R_m = \sqrt{(2/g_m)}/L$; see figures A2c and A2d), above which no solution to the problem exists. Note that for $L_2 \leq L < L_3$, $g_m = g_2$ (figure A2d), while for $L_1 < L < L_r$, R_m is always larger than R_r and R'_r ($g_r < g'_r$; see figures 4 and 5). It must be also noted that for $L_1 < L < L_2$, and for $R'_m < R < R_m$, where $R'_m > 1$ corresponds to the next crossing with the g -axis of the separatrix going towards the spiral point (see figure A2c), a multiplicity of solutions exists for a given value of the pipe radius R (R'_m may be larger or smaller than R_r , depending on m and L ; see figure 4). However, only the lowest branch from the saddle point to $g = g_m$ (figure A2c), is of physical interest, because all the other possible solutions yield unphysical singularities in the flow.

Let's follow increasing L to complete the phase plane picture. For $L = L_3$, the two singular points (68) merge with $g_1 = g_2 = (m-1)/(2-m) = 2/L^2$, which again corresponds to the pipe axis (see figure A2e for $m = 1.2$, where $L_3 \simeq 2.828$). This singular point is no longer a saddle, but the two eigenvalues, which as before coincide with the slopes of the trajectories crossing it, are $a_- = 1-m$ and $a_+ = 0$. The exceptional trajectory crossing the singular point with slope a_- yields a near-axis solution of the form (69), which must be discarded because $a_- < 0$. All the other trajectories reach the singular point with zero slope as

$$G \simeq \frac{1}{2} \left(\frac{2-m}{m-1} \right)^2 (g - g_1)^2, \quad (73)$$

which in physical variables corresponds to

$$\Psi = \frac{W_o}{m} r^m \left(1 + \frac{1}{\ln(c\eta^{-(L/2)^2})} \right)^{m/2}, \quad (74)$$

where c is an arbitrary constant. It can be shown that the singular point is reached with behaviour (73) by infinite trajectories if $g < g_1$, but only by one if

$g > g_1$ (see figure A2e); i.e., the singular point behaves as a node to the "left" of the distinguished trajectory corresponding to $a_- = 1 - m$, which is the only one that reach the singular point with non-zero slope, and as a saddle point to the "right" of it. The only physically meaningful trajectory is, precisely, the exceptional one reaching with zero slope the singular point as (73) from the right ($g > g_1$), implying that solutions only exist for a converging or straight pipe ($R \leq 1$; $R = 1$ corresponds to the singular point itself), in accordance with the trend observed as L approached L_3 .

For $L > L_3$, the two singular points (68) interchange their location: $g_1 < g_2$. The point ($G = 0, g = g_2$) becomes now a saddle and corresponds to the axis of the pipe, with near-axis solution given by

$$\Psi = \frac{W_o L^m}{m 2^{m/2}} g_2^{m/2} r^m (1 + c\eta^{a_{2\pm}})^{m/2}, \quad (75)$$

where $a_{2\pm}$ are given by (70) replacing g_1 by g_2 . Again, only the trajectory with positive slope crossing this point (corresponding to a_{2+} in (75)) is physically meaningful. But now, since $g_2 > 2/L^2$, both branches correspond to a converging or a straight pipe, that going upwards towards infinite, and the other one going downwards towards the singular point ($G = 0, g = 2/L^2$), which is a node for $L_3 < L \leq L_4$, where

$$L_4 = \frac{3 - m}{\sqrt{2(m - 1)}}$$

(plotted in figure 3), and a spiral for $L > L_4$ (see figures A2f and A2g; $R = 1$ corresponds to the lower trajectory going up towards the singular point with $g = 2/L^2$). Whence, no solution for a diverging pipe exists if $L \geq L_3$.

References

- [1] T.B. Benjamin, Theory of the vortex breakdown phenomenon, *J. Fluid Mech.* **14** (1962), 593.
- [2] G.K. Batchelor, *An Introduction to Fluid Dynamics*. Cambridge University Press, 1967. Sec. 7.5.
- [3] J.J. Keller, W. Egli, and J. Exley, Force and loss-free transitions between flow states, *J. Appl. Math. Phys. (ZAMP)* **36** (1985), 854-889.
- [4] P.G. Saffman, *Vortex Dynamics*. Cambridge University Press, 1992. Sec. 14.4.
- [5] J.D. Buntine and P.G. Saffman, Inviscid swirling flows and vortex breakdown, *Proc. R. Soc. Lond. A* **449** (1995), 139-153.
- [6] S. Wang and Z. Rusak, The dynamics of a swirling flow in a pipe and transition to axisymmetric vortex breakdown, *J. Fluid Mech.* **340** (1997), 177-223.
- [7] R. Fernandez-Feria, J. Fernandez de la Mora and A. Barrero, Solution breakdown in a family of self-similar nearly inviscid vortices, *J. Fluid Mech.* **305** (1995), 77-91.
R. Fernandez-Feria, J. Fernandez de la Mora, M. Perez-Saborid and A. Barrero, Conically similar swirling flows at high Reynolds numbers, *Q. J. Mech. Appl. Math.* **52** (1999), 1-53.

- [8] R.L. Long, A vortex in an infinite viscous fluid, *J. Fluid Mech.* **11** (1961), 611-625.
- [9] P.S. Beran and F.E.C. Culik, The role of non-uniqueness in the development of vortex breakdown in tubes, *J. Fluid Mech.* **242** (1992), 491-527.
- [10] J.M. Lopez, On the bifurcation structure of axisymmetric vortex breakdown in a constricted pipe, *Phys. Fluids* **6** (1994), 3683-3693.
- [11] D.L. Darmofal, Comparison of experimental and numerical results for axisymmetric vortex breakdown in pipes, *Comp. Fluids* **25** (1996), 353-371.
- [12] M.G. Hall, A new approach to vortex breakdown. *Proc. Heat Transfer and Fluid Mechanics Institute*, Univ. of California, San Diego 1967, pp. 319-340.
- [13] S.L. Bragg and W.R. Hawthorne, Some exact solutions of the flow through annular cascade actuator discs. *J. Aero. Sci.* **17** (1950), 243-49.
- [14] J.T. Stuart, A critical review of vortex breakdown theory. Proc. 2nd Int. Colloq. Vortical Flows, Baden, Switzerland (1987), 131-153.
- [15] R.E. Spall, T.B. Gatski, and C.E. Grosch, A criterion for vortex breakdown, *Phys. Fluids* **30** (1987), 3434-3440.
- [16] Z. Rusak, K.P. Judd and S. Wang, The effect of small pipe divergence on near critical swirling flows, *Phys. Fluids* **9** (1997), 2273-2285.

R. Fernandez-Feria and J. Ortega-Casanova
Universidad de Málaga
E.T.S. Ingenieros Industriales
29013 Málaga
Spain
(e-mail: ramon.fernandez@uma.es)